*Desalination and Water Treatment*
www.deswater.com

doi: 10.5004/dwt.2017.21633

97 (2017) 175–183
November

# Mefenamic acid stability and removal from wastewater using bentonite-supported nanoscale zero-valent iron and activated charcoal

S. Sulaiman*, T. Shahwan

*Department of Chemistry, Faculty of Science, Birzeit University, Birzeit, P.O. Box 14, Ramallah, West Bank, Palestinian Authority, Tel. +970-2-298-2146; Fax: +970-2-298-2084; emails: ssuliaman@birzeit.edu (S. Sulaiman), tshahwan@birzeit.edu (T. Shahwan)*

Received 14 August 2017; Accepted 11 November 2017

**ABSTRACT**

The low-cost composite, nanoscale zero-valent iron (nZVI) immobilized on bentonite clay (B), was prepared by using the $NaBH_4$ reduction method. The morphology, structure, and composition of B-nZVI were investigated. The use of bentonite as a support material apparently decreased the extent of aggregation and the size of ZVI nanoparticles, thus increasing their surface reactivity and removal efficiency. The B-nZVI composite was used to remove a popular non-steroidal anti-inflammatory drug mefenamic acid (MA) from aqueous solution. For the sake of comparison, the removal of aqueous MA was investigated using activated charcoal and bentonite. Overall, B-nZVI was seen to lead to the best removal efficiency. Batch experiments showed that various parameters, such as time, initial concentration of MA, solid phase dosage, and temperature, can affect the removal of MA. Kinetic studies showed that the removal of MA by B-nZVI correlated well with the pseudo-second-order rate model. The removal process was seen to be endothermic, and the experimental data correlated well with Langmuir isotherm with $Q_{max}$ being 92.6 and 108.7 mg/g for charcoal and B-nZVI, respectively, with a significantly larger binding affinity of MA by B-nZVI.

*Keywords:* Nanoscale; Zero-valent iron; Bentonite; Mefenamic acid; Charcoal

## 1. Introduction

In recent years, one of the most important aspects of environmental research has been the pollution of water from emerging contaminants (ECs), such as endocrine disrupting chemicals, and pharmaceuticals and personal care products [1]. They can be usually found in wastewater only at trace levels but their presence in aquatic systems raises the issue of their harmful effects on human health and the environment [2]. Examples of adverse effects caused by ECs include aquatic toxicity, resistance development in pathogenic bacteria, genotoxicity, and endocrine disruption [1–3].

Recently, the removal of persistent pollutants using nanoscale zero-valent iron (nZVI) has received large attention due to its smaller particle size, larger specific surface area, higher density of reactive surface sites, and greater intrinsic reactivity of surface sites [4,5]. nZVI has become increasingly important in environmental remediation, especially for contaminants such as halogenated organics, heavy metals, pesticides, nitroaromatic compounds, and nitrates [4,5].

Nevertheless, nZVI nanoparticles tend to either react with surrounding media or agglomerate, resulting in significant loss of reactivity [6]. Consequently, since dispersion of nZVI particles is a critical factor to improve their efficiency, various particle-stabilizing strategies have been reported [7–15]. Aggregation phenomena are reported to be considerably reduced when a matrix or a supporting material is used during the synthesis of nZVI. Moreover, iron nanoparticles synthesized in this way tend to exhibit a narrower size distribution, leading to higher activity compared with non-supported systems [16–18]. The synthesis of nZVI has been achieved in the presence of various support materials such as inorganic

* Corresponding author.

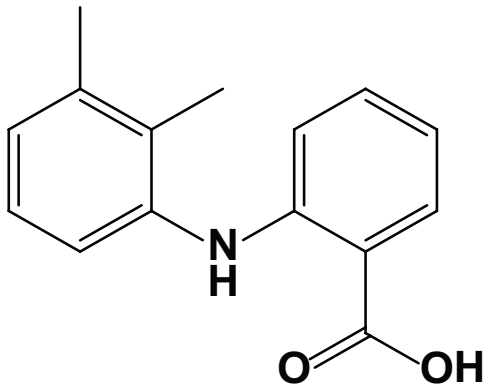


**2-(2,3-dimethylphenyl)aminobenzoic acid**

Fig. 1. Chemical structure of mefenamic acid (MA).

compounds and clay minerals [10,19,20], polymers [16,21–23] or other organic compounds [23], nanostructured carbons [24].

Bentonite is usually composed of montmorillonite and impurities such as quartz and calcite. It is a low-cost clay and efficient adsorbent which has great potential in removing organic and inorganic pollutants from wastewater [25–28]. This clay enjoys a large surface area and high ion exchange capacities, and it is chemically and thermally stable under environmental conditions. Bentonite was used as support material for nZVI to remove $Pb^{2+}$ and $Cr_2O_7^{2-}$ ions [28,29].

Mefenamic acid (MA) is a popular anti-inflammatory drug, which is hard to remove by conventional wastewater treatment technologies. The chemical structure of this drug is (2,3-dimethyl diphenyl)amino-2-carboxylic acid, and the chemical formula is $C_{15}H_{15}NO_2$, and its molar mass is 241.285 g/mol (Fig. 1). It is a member of the anthranilic acid derivatives (or fenamate) class of non-steroidal anti-inflammatory drugs (NSAIDs), which is used to treat mild to moderate pain, including menstrual, and is sometimes used to prevent migraines associated with menstruation [30].

MA is typically prescribed for oral administration. The anti-inflammatory activity of NSAIDs can be attributed to inhibition of the conversion of arachidonic acid to prostaglandins, which are mediators for the inflammation. Modern studies have revealed that in addition to arthritis and pain, cancer and neurodegenerative diseases such as Alzheimer's disease could be potentially treated with NSAIDs due to the inhibition effect on cox-2, which is a recently characterized cyclooxygenase [31,32].

The present study aims at studying the stability of aqueous MA in aqueous solution and sludge, then synthesizing a B-nZVI composite and applying it in the removal of MA under various experimental conditions. For the sake of assessing the efficiency of B-nZVI, its performance is compared with that of a popular adsorbent; activated charcoal. To our knowledge, no similar study exists in literature.

## 2. Materials and methods

### 2.1. Chemicals

Bentonite used in this study was supplied by Sigma Chemical Company Co., Ltd. (Munich, Germany), which had the amount of montmorillonite (wt) <40% and a cation exchange capacity of 32.4 meq/100 g. The chemical composition of the clay is 62.5% $SiO_2$, 18.5% $Al_2O_3$, 1.75% $Fe_2O_3$, 4.25% MgO, 0.95% CaO, and 2.75% $Na_2O$. The reagents of $FeCl_3.6H_2O$, $NaBH_4$, and MA were also obtained from Sigma Chemical Company Co., Ltd. All the chemicals used in this study were of analytical grade and were used without further purification. MA solution of desired concentration was prepared by dissolving the required amount of the drug in a suitable volume of deionized water. Deionized water was used throughout this experiment.

### 2.2. Birzeit University wastewater treatment plant (WWTP) and MA stability

#### 2.2.1. Birzeit University WWTP

A contact stabilization wastewater treatment plant has been used to treat domestic wastewater from all Birzeit University buildings, including the main restaurants and cafeterias as well as various laboratories. At present, Birzeit University has almost 15,000 students and staff, and the amount of sewage collected and treated is about 180 $m^3$/d.

In this process, two aeration tanks are used. One tank is for separate reaeration of the return sludge for at least 4 h before it is permitted to flow into the other aeration tank to be mixed with the primary effluent requiring treatment. For more safety the effluent let to pass through slow sand filter to remove suspended solids, viruses, and microbial pathogens [33].

The wastewater characteristics from Birzeit University are slightly diluted and do not reflect a typical rural domestic sewage. The reason for this is that most of the students stay for a short period of time in the university campus [33].

#### 2.2.2. Physical, chemical, and biological parameters of Birzeit University WWTP sludge

The wastewater was characterized before the experiments according to standard methods [34] listed in Table 1.

#### 2.2.3. Stability study of MA

Stability study for MA in the presence of Birzeit University wastewater treatment plant (WWTP) sludge was performed by adding 1,000 mL of suspended sludge to sorbent under continuous aeration to maintain bacterial growth in the sludge environment. Reproducibility studies were performed in triplicate and the average values were recorded together with standard deviations.

In addition, a stability study of MA was performed with a 100 mg/L solution, prepared by dissolving MA in distilled water adjusted to pH 8.0 using 1 M sodium hydroxide. Samples at specific time intervals: 0, 1, 2, 4, 5, 10, 15, 20, 25, and 30 d were taken, and analyzed by high performance liquid chromatography (HPLC).

### 2.3. Methods

#### 2.3.1. Synthesis of bentonite-supported nZVI

nZVI nanoparticles and bentonite-supported nZVI (B-nZVI) were synthesized using the liquid-phase reduction method in which bentonite acted as a support material as previously reported [9,26,28]:

Table 1
Methods used and wastewater quality parameters measured in the Birzeit University WWTP

| Parameter measured | Instrument used for analysis | Method of analysis | Reference |
|---|---|---|---|
| pH | pH-meter 3320, Jenway | SM#4500-H+(B) (on site) | Direct measurement as manufacturer procedure |
| Conductivity | Conductivity meter 4320, Jenway | 2520-B | APHA [34] |
| Total coliforms and fecal coliforms | Membrane filter method | 9222-B<br>9221-E | APHA [34] |
| Orthophosphate | Automated ascorbic acid reduction | SM# 4500-PF | APHA [34] |
| COD | Hach COD reactor | 5210-B | APHA [34] |
| $BOD_5$ | DO meter – Oxy 197 | 5220-D | |
| $NH_4^+$ | Nesselarization method | 4500A-$NH_3$ | APHA [34] |
| Total bacterial count | Pour plate method after serial dilutions | 9215D | APHA [34] |
| Solids | Gravimetric methods | 2540B<br>2540C<br>2540D | APHA [34] |

$$4Fe^{3+} + 3BH_4^- + 9H_2O \rightarrow 4Fe^0 + 3H_2BO_3^- + 12H^+ + H_2\uparrow$$

B-nZVI was prepared with an iron/bentonite mass ratio of 1:1. For this purpose, 4.84 g of ferric chloride hexahydrate ($FeCl_3.6H_2O$) were dissolved in 50 mL of a mixture of distilled water and absolute ethanol (prepared at a volume ratio of 4:1), and 1.00 g of bentonite was added. The mixture was stirred with a stirring rod for 15 min, and then 100 mL of 0.47 M $NaBH_4$ solution was added dropwise into this mixture and vigorously stirred continuously under nitrogen atmosphere. The mixture's color turned from red brown to light yellow, and then eventually to black.

After all of the $NaBH_4$ solution had been added, the mixture was stirred under the nitrogen atmosphere continuously for another 20 min to completely deplete $NaBH_4$ and $FeCl_3.6H_2O$. Vacuum filtration was employed to collect the B-nZVI particles, and these were quickly rinsed three times with absolute ethanol. This step is necessary to prevent the immediate oxidation of nZVI. Finally, the composite samples were dried at 333 K overnight.

### 2.3.2. Sample characterizations

Fourier transform infrared spectroscopic (FTIR) spectra were obtained with a Fourier transform infrared spectroscope (Nicolet 5700, Thermo Corp., USA). The samples were analyzed directly using ATR-FTIR. An average of five scans was collected for each measurement with a resolution of 4 $cm^{-1}$.

The morphology and nanoparticles distribution of nZVI on bentonite structure were examined using a Philips-FEI XL30 ESEM-TMP (Philips Electronics Co., Eindhoven, Netherlands). Images of samples were recorded at different magnifications at an operating voltage of 20 kV.

X-ray diffraction (XRD) patterns of B-nZVI samples were performed using a Philips-X'Pert Pro MPD (Netherlands) instruments with a high-power Cu K$\alpha$ source ($k$ = 0.154 nm) at 40 kV/40 mA. All samples were scanned from 2$\theta$ = 5°–90° at a scanning rate of 3°/min.

HPLC analyses were performed with high performance liquid chromatography (HPLC-PDA) system consisting of an alliance 2695 HPLC (Waters: Milford, MA, USA), and a waters Micromass® Masslynx™ detector with photodiode array (Waters 2996). Data acquisition and control were carried out using Empower™ software (Waters). Analytes were separated on a 4.6 mm × 150 mm C18 XBridge® column (5 μm particle size) used in conjunction with a 4.6 mm × 20 μm XBridge™ C18 guard column. Microfilter was used with 0.45 μm (Acrodisc® GHP, Waters), pH meter model HM-30G: TOA electronics™ was used in this study to measure the pH value for the samples. The $C_{18}$ (1 g) cartridges 6cc single use for general laboratory usage were purchased from Waters Company (Milford, MA, USA).

### 2.3.3. Batch experiments

Batch-type experiments were performed to study the removal of the MA by both adsorbents (B-nZVI and activated charcoal) under various experimental conditions such as time, concentration, adsorbent dose, and temperature. Distilled water was used to prepare the solutions and the initial pH was adjusted to 8.0 by using 1 M sodium hydroxide. The removal experiments of MA were realized by placing 100 mL from each solution into a 250 mL Erlenmeyer flask (Darmstadt, Germany), then adding 0.1 g of the adsorbent to each flask, separately. The flask was then placed on a shaker for 180 min. The effect of concentration was studied at the initial drug concentrations 5, 10, 50, 100, and 200 mg/L. The effect of time was studied at 100 mg/L drug concentration and the samples were taken and analyzed at different time intervals 0, 5, 10, 20, 30, 40, 50, 60, 80, 100, 120, 150, and 180 min. The effect of adsorbent dose was studied in the range of 0.1–1.0 g/L, and the effect of temperature was studied in the range of 15°C–55°C.

At the end of contact periods, each sample was centrifuged for 5 min, and filtered using 0.45 μm filters. In each case 20 μL of the filtered solution were injected into the HPLC and the peak area of MA was recorded.

The percentage removal of MA was calculated using the well-known mass balance equation:

$$R(\%) = \frac{C_0 - C_t}{C_0} \times 100\% \quad (1)$$

where $R$(%) is the percentage removal, $C_0$ (mg/L) is the initial liquid concentration of MA, and $C_t$ (mg/L) is the liquid concentration of MA at a specific time $t$.

Blank experiments of MA were conducted as parallel control as well. Experimental results could have made negligible any loss of the pollutant adsorbed on the glassware wall and/or self-degraded. All these experiments were undertaken in quadruplicate.

#### 2.3.4. Calibration curves

Linearity of the proposed analytical method was verified by analyzing standard solutions in the range of 0.1–200 mg/L for MA. The calibration curve was obtained with a determination coefficient ($R^2$) of 0.9998. The repeatability of triplicate subsequent injections was ranging from 98.5% to 99.5%, depending on the sample concentration.

## 3. Results and discussion

### 3.1. Wastewater characteristics and stability of MA

Table 2 summarizes the chemical, physical, and biological characteristics of wastewater collected from Birzeit University WWTP activated sludge reservoir. Careful inspection of Table 2 reveals that the sludge is rich in N and P with medium values of biological oxygen demand (BOD), chemical oxygen demand (COD), total dissolved solids (TDS), settable solids, and high bacterial count. These values are expected since the analyzed samples were taken from the aeration tank in the activated sludge unit within the wastewater treatment plant.

Table 2 also demonstrates that this wastewater contains medium amounts of suspended solids and large populations of bacteria. Birzeit University activated sludge was found to contain Enterobacter species: *Enterococcus faecalis, Escherichia coli, Enterobacter sakazakii, Pseudomonas aeruginosa, Klebsiella pneumonia, Enterobacter cloacae, Enterobacter aerogenes, Salmonella* spp., *Comamonadaceae, Pseudomonadaceae, Flavobacteriaceae, Verrucomicrobiaceae, Streptococcus, Neisseriaceae,* and *Leptotrichiaceae.* Moreover, high values of electrical conductivity and total dissolved solids are typical of municipal wastewaters and should be reduced if WWTP effluents are to be reused for crop irrigation purposes.

Table 2
Physical, chemical, and biological parameters of wastewater

| Parameters | Results |
|---|---|
| pH | 8.22 ± 0.01 |
| Conductivity, μSm/cm | 502 ± 8 |
| Temperature, °C | 17.9 ± 0.2 |
| Turbidity, NTU | 5,000 ± 200 |
| DO, mg/L | 1.59 ± 0.01 |
| TS, mg/L | 1,040 ± 20 |
| TDS, mg/L | 346 ± 30 |
| Settable solids, mg/L | 210 ± 5 |
| TSS, mg/L | 690 ± 20 |
| BOD, mg/L | 370 ± 50 |
| COD, mg/L | 180 ± 50 |
| $NH_4$–N, mg/L | 23.7 ± 0.4 |
| $PO_4$–P, mg/L | 6.3 ± 0.2 |
| FC (*E. coli*), cfu/100 mL | $2.9 \times 10^5 \pm 1.5 \times 10^5$ |
| TC, cfu/100 mL | $3.5 \times 10^6 \pm 3.0 \times 10^6$ |
| TAC, cfu/100 mL | $1.6 \times 10^7 \pm 1.3 \times 10^7$ |

Note: DO, dissolved oxygen; FC, fecal coliform; TC, total coliform; TS, total solids; TDS, total dissolved solids; TSS, total suspended solids; TAC, total aerobic count.

The monitoring of MA stability in pure water and in Birzeit University sludge revealed no degradation during more than 1 month of standing at ambient temperature. These findings indicate that MA is resistant to water hydrolysis and bacterial degradation [35].

Literature survey on the stability and biodegradation of MA indicates that in mammals, the drug undergoes metabolism by CYP2C9 to the metabolite 3-hydroxymethyl MA which further undergoes oxidation to a 3-carboxy mefenamic acid. MA can also be glucuronidated directly, and the fecal route of elimination may account for up to 20% of the dose, mainly in the form of unconjugated 3-carboxy mefenamic acid MA. Both renal and hepatic excretions are significant pathways of elimination [35,36].

It was reported that treating MA with white rot fungus *Phanerochaete sordida* YK-624. MA can decrease its concentration by about 90% after 6 d of treatment. Moreover, mass spectrometric and $^1$H NMR analyses showed four metabolites of MA characterized as 3′-hydroxymethyl mefenamic acid (monohydroxylated mefenamic acid (MFA)), 3′-hydroxymethyl-5-hydroxymefenamic acid (dihydroxylated MFA), 3′-hydroxymethyl-6′-hydroxymefenamic acid (dihydroxylated MFA), and 3′-carboxy mefenamic acid [37].

### 3.2. nZVI characterization

Naturally, iron is usually found in its thermodynamically stable oxide forms under normal conditions, and ZVI is unstable and gets oxidized very easily. This fact illustrates the high chemical reactivity of metallic iron particles which leads to its high capability in converting various contaminants to less toxic forms [14,16].

nZVI is a manufactured material which is well-known to exhibit a typical core–shell structure. The core consists of zero valent or metallic iron ($Fe^0$), while the shell is composed of mixed valent iron (Fe(II) and Fe(III)) oxides which are formed as a result of oxidation of the nanoparticles. Current research results show that nZVI possesses excellent electron donating properties, which makes it a versatile remediation material [38]. By virtue of its core–shell structure, nZVI can fix the contaminants through a redox mechanism and/or a sorption mechanism. The core forms an electron source for the redox reactions with many types of organic/inorganic pollutants, whereas the oxide shell provides the sites for chemical complex reactions (chemisorptions) and electrostatic interactions.

Due to strong magnetic dipoles, ZVI nanoparticles form chain-like aggregates. When the nanoparticles agglomerate, they have a continuous oxide shell but the metallic cores are separated by thinner interfacial oxide layers. The oxide layer is amorphous and disordered, owing to the extremely small radii of the nanoparticles, which hinders crystalline formation [39,40]. It is suggested that the oxide layer protects the core

of the nanoparticles against further oxidation and provides a means for the transport of mass and charge across it [40].

The defective and disordered nature of the oxide shell renders it potentially more reactive compared with a simple passive oxide layer formed on bulk iron material [39]. This layer plays an important role in the charge transfer from the nanoparticle core to the sequestrated contaminant on the external surface. It has semiconductor properties [5,41], and so charge transfer is relatively superficial due to small thickness and the presence of defective sites which can facilitate reduction of contaminants to occur.

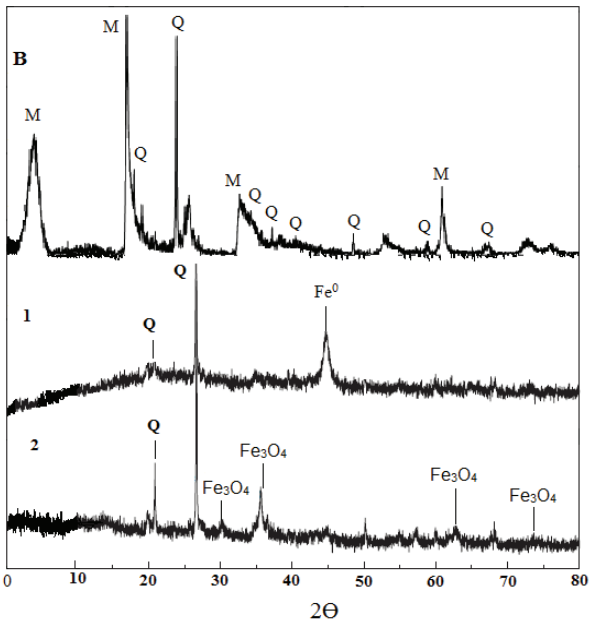


Fig. 2. XRD patterns: (B) bentonite; (1) B-nZVI before reaction; and (2) B-nZVI after reaction.

nZVI and B-nZVI used in this study were characterized using XRD, scanning electron microscopy (SEM), transmission electron microscopy (TEM) and FTIR. The XRD results are shown in Fig. 2. The occurrence of nZVI in the sample is marked by the basic reflection at 45°. The nZVI samples usually suffer from low crystallinity. One important reason is the presence of boron (originating from the reducing agent $NaBH_4$) in the lattice of the metal nanoparticles. The figure also shows the reflections of montmorillonite (*M*) – the main component of bentonite – in addition to quartz (*Q*) which exists as an impurity in the bentonite sample. The montmorillonite reflections disappeared from the XRD diagram of B-nZVI, possibly indicating that the clay experienced exfoliation upon incorporating Fe nanoparticles in-between its layers. Fig. 2 also provides an XRD pattern of nZVI after the removal of aqueous MA. It is clear that the sample has undergone massive oxidation as evident by the disappearance of $Fe^0$ reflection and the appearance of $Fe_3O_4$ (magnetite) reflections.

Typical SEM images of a fresh sample of nZVI, B-nZVI, and bentonite are demonstrated in Fig. 3. Raw bentonite appears as large flocs with leafy-like lamellas, and plenty of small ravines among different interlaminations as shown in Fig. 3(a). On the other hand, Figs. 3(b) and (c) show that synthesized nZVI possess typical chain-like aggregates, composed of spherical nanoparticles. In B-nZVI, partial decrease in the nanoparticles aggregation seems to occur and the aggregated and dispersed nanoparticles seem to accumulate

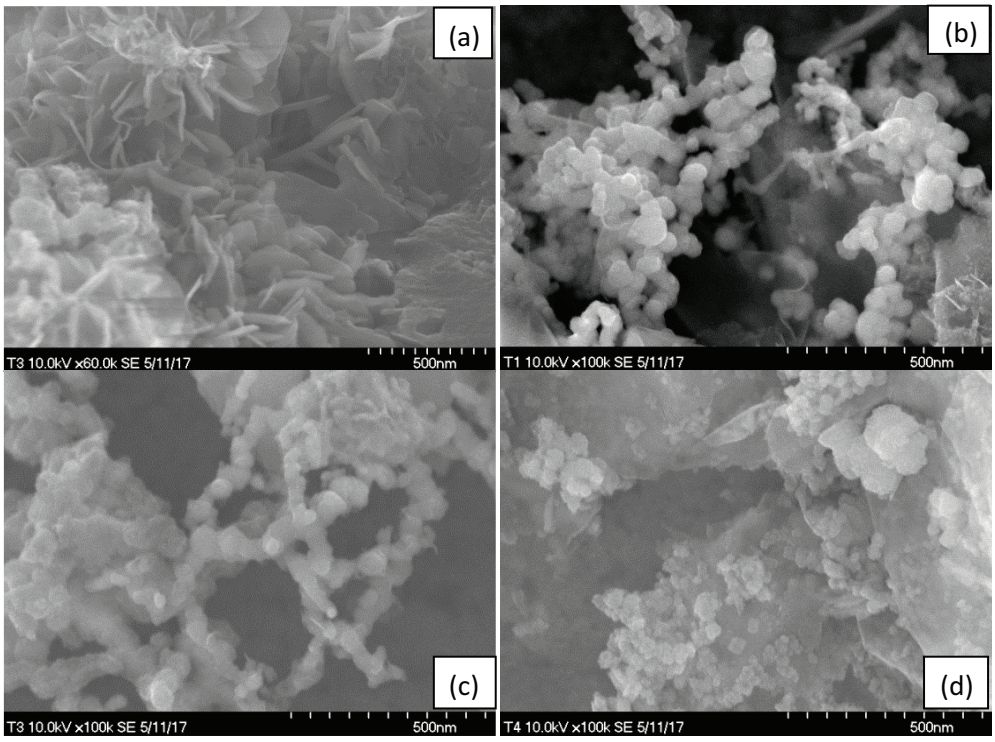


Fig. 3. SEM images of various materials: (a) bentonite; (b) and (c) nZVI before reaction; and (d) B-nZVI after reaction.

at the internal structure of the clay. Fig. 3(d) demonstrates that nZVI morphology has largely changed suggesting that the material undergo massive oxidation after the removal of the contaminant, which is confirmed by XRD results given above.

The partial dispersion of nZVI on clay sheets is evident in the TEM image shown in Fig. 4. The average size of individual nZVI dispersed on bentonite structure seems to vary in the range of 40–100 nm.

The FTIR spectra for natural bentonite and B-nZVI were obtained in the range of 400–4,000 $cm^{-1}$. In Fig. 5, the bands at 1,020 and 915 $cm^{-1}$ arise from the vibrations of Si–O and Al–O, respectively [42]. The bands at 995 $cm^{-1}$ are assigned to Si–O vibrations. The band observed at 1,638 $cm^{-1}$ is due to H–O–H stretching vibration bands of water molecule weakly hydrogen bonded to the Si–O surface in B, while the bands at 3,626 $cm^{-1}$ refer to the presence of Al–O–H groups. The bands at 520 and 437 $cm^{-1}$ are due to Si–O–Al (octahedral) and Si–O–Si bending vibrations, respectively [43]. The deep band at around 1,018 $cm^{-1}$ represents the stretching of Si–O in the Si–O–Si groups of the tetrahedral sheet. In addition, the bands at 458, 519, 797, 915, and 1,020 $cm^{-1}$ correspond to the Fe–O stretching possibly originating from iron oxide [42]. These features agreed well with the bands from the nZVI spectra indicating that nZVI in B-nZVI were partially oxidized. The Si–O stretching vibration at around 995 $cm^{-1}$ shifts to 1,020 $cm^{-1}$ suggesting some structural changes in the clay. No new band was observed after B-nZVI was reacted with MA. This is possibly because most of the adsorbed MA concentration (or the concentration of its degradation products) is below the detection limit of FTIR.

### 3.3. Comparison of removal efficiency of MA using various materials

#### 3.3.1. Effect of time

The effect of time on the removal of MA by B-nZVI was studied at an initial drug concentration of 100 mg/L. For the sake of comparison, the reaction was also conducted using the conventional adsorbent, activated charcoal, in addition to bentonite. The results which are given in Fig. 6 suggest that B-nZVI demonstrated the best performance, followed by charcoal, and finally bentonite, which showed very low removal percentages. Less than 1 h is seen to be needed to approach equilibrium when B-nZVI is used, with the percentage removal amounting to about 60% at the applied concentration.

Given the low removal capacity of bentonite toward MA, it can be concluded that nZVI played the dominant role in the removal of MA using B-nZVI. Bentonite seems to be acting mainly as a dispersant of nZVI with limited sorption efficiency toward MA [10,12,25]. These results are consistent with earlier results obtained for kaolin-supported nZVI in the removal of Pb(II) [11], and bentonite-supported nZVI for the removal of Cr(V) from aqueous solution [12].

The kinetic data of MA removal by B-nZVI and activated charcoal were tested using a modified pseudo-second-order rate equation, given as [44]:

$$\frac{t}{Q} = \frac{1}{Q_m C_0 k_2} + \frac{1}{Q_m} t \tag{2}$$

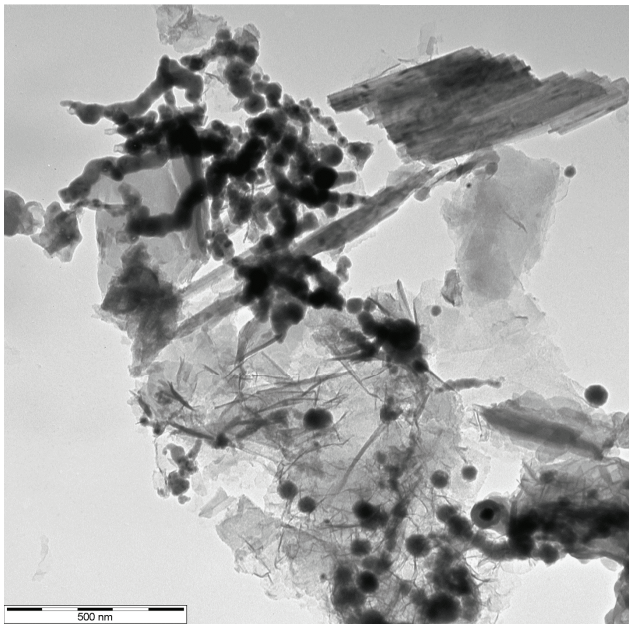


Fig. 4. TEM image of B-nZVI.

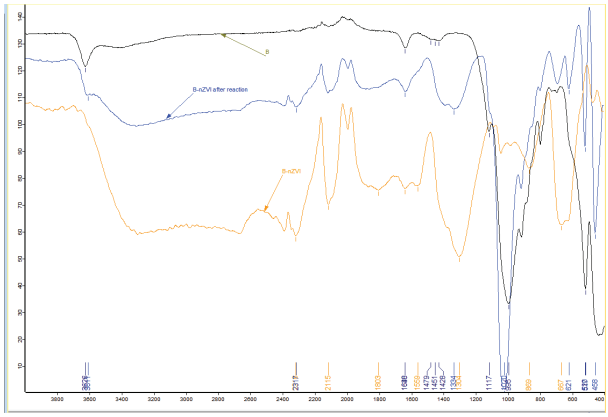


Fig. 5. FTIR spectra of: (a) bentonite; (b) B-nZVI; and (c) B-nZVI after reaction.

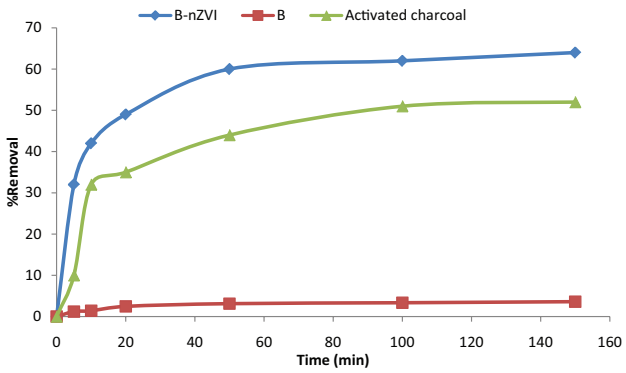


Fig. 6. Percentage removal of mefenamic acid, from dispersions by B-nZVI, activated charcoal, and bentonite as a function of time, $C$ = 100 mg/L, dose = 0.1 g/L, and $T$ = 25°C.

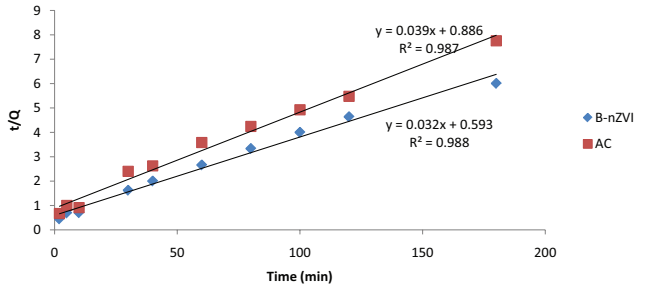


Fig. 7. Kinetic plots of MA removal by B-nZVI and activated charcoal using a modified pseudo-second-order equation.

where $Q_m$ stands for the maximum amount of the adsorbate, $C_0$ its initial concentration, and $k_2$ is the rate constant. Both $Q_m$ and $k_2$ can be obtained from the slope and the intercept of the linear plots of $t/Q$ vs. $t$.

The linear plots of the data are given in Fig. 7 for MA removal by B-nZVI and charcoal. Under the specified conditions, the obtained values of $Q_m$ were 31.06 mg/g for B-nZVI and 25.4 mg/g for charcoal, while the $k_2$ values were $5.4 \times 10^{-4}$ L/min mg and $4.4 \times 10^{-4}$ L/min mg, respectively. These values show that B-nZVI has higher removal capacity of MA than charcoal, and that the removal process is also faster in the case of B-nZVI.

### 3.3.2. Effect of initial concentration

The extent of removal of MA was studied as a function of drug concentration. Table 3 summarizes the percentage removal of MA using B-nZVI, bentonite, and activated charcoal. Under the specified conditions, B-nZVI showed the best performance at different concentrations, with bentonite showing very small removal percentages, thus suggesting that nZVI is the composite component responsible for the observed removal of MA. It is also clear that under the studied conditions, the percentage removal of MA increased as the initial concentration was increased in the cases of the three sorbents.

The experimental data were analyzed by Langmuir isotherm, given by the equation [1]:

$$\frac{C_e}{Q_e} = \frac{1}{(kQ_{\max})} + \frac{C_e}{Q_{\max}} \quad (3)$$

where $C_e$ (mg/L) is equilibrium concentration of MA, $Q_e$ (mg/g) is equilibrium mass of adsorbed MA per gram of sorbent, $k$ (L/mg) is Langmuir binding constant, and $Q_{\max}$ (mg/g) is maximum mass of drug removed per gram of adsorbent.

The experimental data for the effect of concentration on the removal of MA by B-nZVI and activated charcoal were found to fit the Langmuir isotherm model (Eq. (3)), with $R^2$ being greater than 0.99 for both cases (Fig. 8) MA. The Langmuir constants ($k$ and $Q_{\max}$) were calculated and presented in Table 4. Inspection of Table 4 reveals that the B-nZVI has larger $k$ and $Q_{\max}$ than activated charcoal, thus rendering the former as a more effective material for removal of MA than the latter, in terms of removal capacity and affinity.

Table 3
Percentage removal of mefenamic acid by B-nZVI, bentonite, and activated charcoal as a function of initial concentration after incubation for 3 h at a temperature of 25°C, B-nZVI dosage 0.1 g/L

| Initial concentration (mg/L) | Percentage removal (%) initial concentration | | |
|---|---|---|---|
| | B-nZVI | Bentonite | Activated charcoal |
| 5 | 32 ± 0.5 | 1.2 ± 1 | 10 ± 0.5 |
| 10 | 42 ± 0.6 | 1.4 ± 1 | 32 ± 0.5 |
| 20 | 49 ± 1 | 2.5 ± 1 | 35 ± 1 |
| 50 | 60 ± 1 | 3.1 ± 1 | 44 ± 1 |
| 100 | 62 ± 1 | 3.3 ± 1 | 52 ± 1 |
| 200 | 64 ± 1 | 3.6 ± 1 | 54 ± 1 |

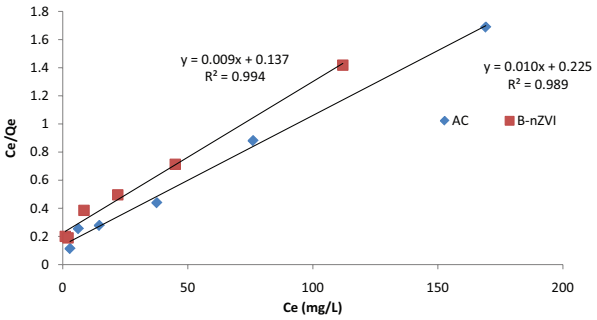


Fig. 8. Langmuir isotherms for the removal of MA by B-nZVI (¢) and by activated charcoal (®) (pH 8.0 and $T$ = 25°C).

Table 4
Langmuir isotherm parameters ($k$ and $Q_{\max}$) and the correlation coefficient ($R^2$) values obtained from the removal of MA on B-nZVI and activated charcoal

| Adsorbents | Langmuir | | |
|---|---|---|---|
| | $k$ (L/mg) | $Q_{\max}$ (mg/g) | $R^2$ |
| B-nZVI | 0.0669 | 108.7 | 0.9943 |
| Charcoal | 0.0465 | 92.6 | 0.9899 |

### 3.3.3. Effect of dose

The effect of MA removal was studied at different loadings of B-nZVI, namely 0.1, 0.25, 0.5, 0.75, and 1.0 g/L. The corresponding removal percentages are shown in Fig. 9. As can be seen from the figure a dose of 0.25 g/L B-nZVI would be enough to achieve a complete drug removal under the studied conditions. Beyond this amount the percentage removal did not change suggesting the availability of enough surface sites to lead to complete removal of MA.

As a further test of the effect of sorbent dose at different MA concentrations on its removal by B-nZVI, the experiments were conducted at higher MA initial concentrations, namely 50, 100, 300, 500, and 1,000 mg/L, while increasing the sorbent loading to 0.25 g/L. The results shown in Fig. 10 suggest that up to 100 mg/L MA concentration, a complete removal is achievable. Beyond this, the percentage removal decreases as initial concentration increases. This trend is the

opposite of that observed at the lower concentration range given above, and underlines the importance of the concentration range on the extent of MA removal. Given the high initial concentrations of MA, the results can be attributed to the unavailability of sufficient number of active sites because a fixed quantity of sorbent dose was used [45].

### 3.3.4. Effect of temperature

The influence of temperature on the removal of MA by B-nZVI was investigated in the range of 15°C–55°C, and the obtained results are shown in Fig. 11. It can be seen that the increase in temperature increased the removal of MA from 70.0% at 15°C to 99.0% at 25°C. Beyond this temperature, the removal appears to stay almost complete. This endothermic behavior indicates that temperature increases the chemical potential of MA molecules in the solution, thus increasing their mobility and yielding complete removal.

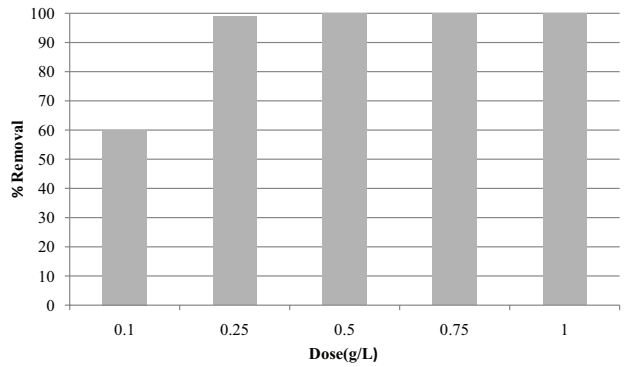


Fig. 9. Effect of B-nZVI dose (g/L) on percentage removal of MA at $C_0$ = 100 mg/L, pH = 6, time = 3 h, and $T$ = 25°C.

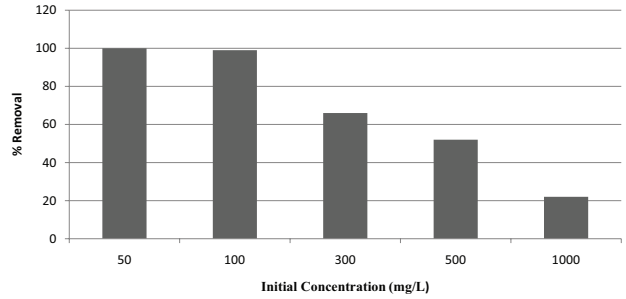


Fig. 10. Effect of initial concentration on percentage removal of MA at pH = 6, dose = 0.25 g/L, time = 3 h, and $T$ = 25°C.

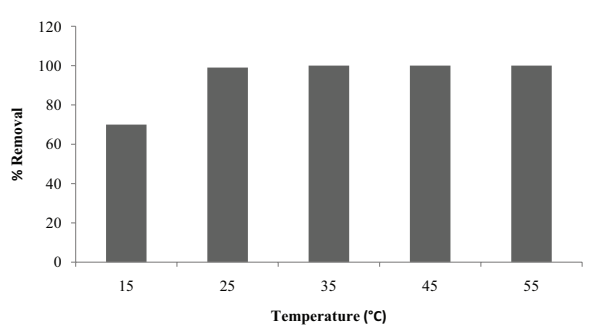


Fig. 11. Effect of temperature on percentage removal of MA at pH = 6, $C_0$ = 100 mg/L, $m$ = 0.25 g/L, and time = 3 h.

## 4. Conclusions

Iron nanoparticles employed in this study consisted mainly of ZVI. It has been shown that bentonite has the potential to act as a dispersant and stabilizer during the synthesis of B-nZVI, which decreased aggregation and enhanced activity of nZVI.

MA was stable in distilled water and in Birzeit University sludge up to 30 d. Batch experiments showed that various parameters such as time, initial concentration of MA, sorbent dosage, and temperature have various effects on the removal process, but a complete removal of the drug is possible under a wide range of conditions.

The obtained data correlated well with pseudo-second-order rate equation and Langmuir isotherm. The comparative study of B-nZVI and activated charcoal indicated that the former possesses higher removal capacity and faster removal kinetics.

It is proposed that the degradation mechanism of MA using B-nZVI may include adsorption and redox routes, which may lead to adsorption of MA to B-nZVI, formation of Fe(II)–MA complex, and/or cleavage of NH secondary amine bond of MA. Further studies are required to shed more light on the removal mechanism.

Overall, the results suggest that incorporation of B-nZVI filters in secondary wastewater treatment plants could be promising in removing MA from the aquatic environment.

## Acknowledgments

The financial support of this research from the Scientific Research Committee at Birzeit University is gratefully acknowledged. We thank our colleagues from Birzeit University: Assem M. Mobarak, Azmi N. Dudin, and Shadi H. Kaibni for their technical support that greatly assisted the research. The authors thank Montaha Masri (Ulm University) for her assistance in the XRD, SEM, and TEM characterization of iron nanomaterials.

## References

[1] S. Sulaiman, M. Khamis, S. Nir, F. Lelario, L. Scrano, S.A. Bufo, R. Karaman, Stability and removal of dexamethasone sodium phosphate from wastewater using different techniques, Environ. Technol., 35 (2014) 1945–1955.
[2] S. Sulaiman, M. Khamis, S. Nir, L. Scrano, S.A. Bufo, R. Karaman, Diazepam stability in wastewater and removal by advanced membranes technology, activated carbon and micelle–clay complex, Desal. Wat. Treat., 57 (2016) 3098–3106.
[3] S. Sulaiman, M. Khamis, S. Nir, F. Lelario, L. Scrano, S.A. Bufo, R. Karaman, Stability and removal of spironolactone from wastewater, J. Environ. Sci. Health, Part A, 50 (2015) 1127–1135.
[4] J. Theron, J.A. Walker, T.E. Cloete, Nanotechnology and water treatment: applications and emerging opportunities, Crit. Rev. Environ. Sci. Technol., 34 (2008) 43.
[5] X.Q. Li, D.W. Elliott, W.X. Zhang, Zero-valent iron nanoparticles for abatement of environmental pollutants: materials and engineering aspects, Crit. Rev. Solid State Mater. Sci., 31 (2006) 111–122.

[6] P. He, D.Y. Zhao, Preparation and characterization of a new class of starch-stabilized bimetallic nanoparticles for degradation of chlorinated hydrocarbons in water, Environ. Sci. Technol., 39 (2005) 3314–3320.
[7] S.M. Ponder, J.G. Darab, T.E. Mallouk, Remediation of Cr(VI) and Pb(II) aqueous solutions using supported, nanoscale zero-valent iron, Environ. Sci. Technol., 34 (2000) 2564–2569.
[8] Y. Xu, D. Zhao, Reductive immobilization of chromate in water and soil using stabilized iron nanoparticles, Water Res., 41 (2007) 2101–2108.
[9] T. Shahwan, A. Üzüm, A. Eroglu, I. Lieberwirth, Synthesis and characterization of bentonite/iron nanoparticles and their application as adsorbent of cobalt ions, Appl. Clay Sci., 47 (2010) 257–262.
[10] C. Üzüm, T. Shahwan, A.E. Eroglu, K.R. Hallam, T.B. Scott, I. Lieberwirth, Synthesis and characterization of kaolinite-supported zero-valent iron nanoparticles and their application for the removal of aqueous $Cu^{2+}$ and $Co^{2+}$ ions, Appl. Clay Sci., 43 (2009) 172–181.
[11] X. Zhang, S. Lin, X.Q. Lu, Z.L. Chen, Removal of Pb(II) from water using synthesized kaolin supported nanoscale zero-valent iron, Chem. Eng. J., 163 (2010) 243–248.
[12] L.N. Shi, X. Zhang, Z.L. Chen, Removal of chromium (VI) from wastewater using bentonite-supported nanoscale zero-valent iron, Water Res., 45 (2011) 866–892.
[13] M. Stratmann, J. Muller, The mechanism of the oxygen reduction on rust covered metal substrates, Corros. Sci., 36 (1994) 327–359.
[14] C. Noubactep, S. Caré, R.A. Crane, Nanoscale metallic iron for environmental remediation: prospects and limitations, Water Air Soil Pollut., 223 (2012) 1363–1382.
[15] M.M. Scherer, S. Richter, R.L. Valentine, P.J.J. Alvarez, Chemistry, microbiology of permeable reactive barriers for in situ groundwater cleanup, Crit. Rev. Microbiol., 26 (2000) 221–264.
[16] S.M. Ponder, J.G. Darab, J. Bucher, D. Caulder, I. Craig, L. Davis, N. Edelstein, W. Lukens, H. Nitsche, L.F. Rao, D.K. Shuh, T.E. Mallouk, Surface chemistry and electrochemistry of supported zerovalent iron nanoparticles in the remediation of aqueous metal contaminants, Chem. Mater., 13 (2001) 479–486.
[17] H. Zhang, Z.H. Jin, L. Han, C.H. Qin, Synthesis of nanoscale zero-valent iron supported on exfoliated graphite for removal of nitrate, Trans. Nonferrous Met. Soc. China, 16 (2006) 345–349.
[18] L. Li, M. Fan, R. Brown, J. Van Leeuwen, J. Wang, W. Wang, Y. Song, P. Zhang, Synthesis, properties and environmental applications of nanoscale iron-based materials: a review, Crit. Rev. Environ. Sci. Technol., 36 (2006) 405–431.
[19] Y. Li, Z. Jin, T. Li, S. Li, Removal of hexavalent chromium in soil and groundwater by supported nano zero-valent iron on silica fume, Water Sci. Technol., 63 (2011) 2781–2787.
[20] J. Zhan, T. Zheng, G. Piringer, C. Day, G.L. McPherson, Y. Lu, K. Papadopoulos, V.T. John, Transport characteristics of nanoscale functional zero valent iron/silica composites for in situ remediation of trichloroethylene, Environ. Sci. Technol., 42 (2008) 8871–8876.
[21] H. Kim, H.J. Hong, Y.J. Lee, H.J. Shin, J.W. Yang, Degradation of trichloroethylene by zero-valent iron immobilized in cationic exchange membrane, Desalination, 223 (2008) 212–220.
[22] D.E. Meyer, K. Wood, L.G. Bachas, D. Bhattacharyya, Degradation of chlorinated organics by membrane-immobilized nanosized metals, Environ. Prog., 23 (2004) 232–242.
[23] H. Kim, H.-J. Hong, J. Jung, S.-H. Kim, J.-W. Yang, Degradation of trichloroethylene (TCE) by nanoscale zero-valent iron (nZVI) immobilized in alginate bead, J. Hazard. Mater., 176 (2010) 1038–1043.
[24] X. Ling, J. Li, W. Zhu, Y. Zhu, X. Sun, J. Shen, W. Han, L. Wang, Synthesis of nanoscale zero-valent iron/ordered mesoporous carbon for adsorption and synergistic reduction of nitrobenzene, Chemosphere, 87 (2012) 655–660.
[25] E. Eren, Adsorption performance and mechanism in binding of azo dye by raw bentonite, Clean Soil Air Water, 38 (2010) 758–763.
[26] V.K. Gupta, Suhas, Application of low-cost adsorbents for dye removal – a review, J. Environ. Manage., 90 (2009) 2313–2342.
[27] M. Galamboš, P. Suchánek, O. Rosskopfová, Sorption of anthropogenic radionuclides on natural and synthetic inorganic sorbents, J. Radioanal. Nucl. Chem., 293 (2012) 613–633.
[28] M. Galamboš, A. Krajňák, O. Rosskopfová, E. Viglašová, R. Adamcová, P. Rajec, Adsorption equilibrium and kinetic studies of strontium on Mg-bentonite, Fe-bentonite and illite/smectite, J. Radioanal. Nucl. Chem., 298 (2013) 1031–1040.
[29] M. Rafatullah, O. Sulaiman, R. Hashim, A. Ahmad, Adsorption of methylene blue on low-cost adsorbents: a review, J. Hazard. Mater., 177 (2010) 70–80.
[30] T. Pringsheim, W.J. Davenport, D. Dodick, Acute treatment and prevention of menstrually related migraine headache: evidence-based review, Neurology, 70 (2008) 1555–1563.
[31] K. Taotao, J. Xiaohui, Z. Limei, Y. Mei, D. Ming, L. Pingli, J. Xiaomin, Removal of methyl orange from aqueous solutions using a bentonite modified with a new Gemini surfactant, Appl. Clay Sci., 54 (2011) 184–187.
[32] F.P. Trinus, N.A. Mokhort, L.M. Yagupolskii, A.G. Fadeicheva, V.S. Danilenko, T.K. Ryabukha, Y.A. Fialkov, L.M. Kirichek, Mefenamic acid A nonsteroid anti-inflammatory agent, Pharm. Chem. J., 11 (1977) 1706–1711.
[33] R. Al-Saed, O. Zimmo, Process performance evaluation of the contact stabilization system at Birzeit University, Int. J. Environ. Pollut., 21 (2004) 511–517.
[34] American Public Health Association, Standard Methods for the Examination of Water and Wastewater, 21th ed., APHA, Washington, D.C., USA, 2005.
[35] G.D. Champion, G.G Graham, Pharmacokinetics of non-steroidal anti-inflammatory agents, Aust. N.Z. J. Med., 8 (1978) 94–100.
[36] R.A. McGurk, R.P. Remmel, V.P. Hosagrahara, D. Tosh, B. Burchell, Reactivity of mefenamic acid 1-o-acyl glucuronide with proteins in vivo and ex vivo, Drug Metab. Dispos., 24 (1996) 842–849.
[37] T. Hata, S. Kawai, H. Okamura, T. Nishida, Removal of diclofenac and mefenamic acid by the white rot fungus *Phanerochaete sordida* YK-624 and identification of their metabolites after fungal transformation, Biodegradation, 21 (2010) 681–689.
[38] W. Stumm, J.J. Morgan, Aquatic Chemistry, 3rd ed., Wiley, New York, 1996.
[39] C.M. Wang, D.R. Baer, J.E. Amonette, M.H. Engelhard, J. Antony, Y. Qiang, Morphology and electronic structure of the oxide shell on the surface of iron nanoparticles, J. Am. Chem. Soc., 131 (2009) 8824–8832.
[40] E.E. Carpenter, S. Calvin, R.M. Stroud, V.G. Harris, Passivated iron as core-shell nanoparticles, Chem. Mater., 15 (2003) 3245–3246.
[41] B.A. Balko, P.G. Tratnyek, Photoeffects on the reduction of carbon tetrachloride by zero-valent iron, J. Phys. Chem. B, 102 (1998) 1459–1465.
[42] P. Yuan, F. Annabi-Bergaya, Q. Tao, M. Fan, Z. Liu, J. Zhu, H. He, T. Chen, Oxidation of tetrahydrofuran to butyrolactone catalyzed by iron-containing clay, J. Colloid Interface Sci., 324 (2008) 142–149.
[43] A. Tabak, B. Afsin, B. Caglar, E. Koksal, Characterization and pillaring of a Turkish bentonite (Resadiye), J. Colloid Interface Sci., 313 (2007) 5–11.
[44] T. Shahwan, Sorption kinetics: obtaining a pseudo-second order rate equation based on a mass balance approach, J. Environ. Chem. Eng., 2 (2014) 1001–1006.
[45] Z. Fang, J. Chen, X. Qiu, W. Cheng, L. Zhu, Effective removal of antibiotic metronidazole from water by nanoscale zero-valent iron particles, Desalination, 268 (2011) 60–67.